# Probing magnetic ordering in multilayers using soft x-ray resonant magnetic scattering

C. H. Marrows,* P. Steadman,† A. C. Hampson, L.-A. Michez, and B. J. Hickey
*School of Physics and Astronomy, E. C. Stoner Laboratory, University of Leeds, Leeds LS2 9JT, United Kingdom*

N. D. Telling
*Daresbury Laboratory, Warrington, Cheshire. WA4 4AD, United Kingdom*

D. A. Arena
*National Synchrotron Light Source, Brookhaven National Laboratory, Upton, New York 11973-5000, USA*

J. Dvorak
*Department of Physics, Montana State University, Bozeman, Montana 59717, USA*

S. Langridge
*Rutherford Appleton Laboratory, Chilton, Didcot, Oxon OX11 0QX, United Kingdom*
(Received 23 July 2004; revised manuscript received 22 December 2004; published 12 July 2005)

We have carried out resonant magnetic x-ray scattering from Co/Ru multilayers with weak antiferromagnetic coupling. We have measured hysteresis loops at different points in reciprocal space (specular or diffuse, integer or half-order peaks), which reveal a rich variety of different shapes. These arise from different degrees of mixing of the scattering arising from the field dependence of the order parameters describing the degree of ferromagnetic, antiferromagnetic correlations in the sample, with the off-specular measurements giving information about their lateral extent. We make a comparison with macroscopic measurements that give information about the degree of different forms of magnetic order averaged over the whole sample in real space.

DOI: 10.1103/PhysRevB.72.024421 PACS number(s): 75.70.Cn, 78.70.Ck, 75.60.−d

## I. INTRODUCTION

One of the main themes in contemporary research in magnetism is the study of ultrathin films and multilayer heterostructures which display a variety of fascinating physical properties[1] as well as being of tremendous technological importance in hard disk media,[2] read heads,[3] magnetic RAM,[4] and other spintronic applications.[5] These systems contain numerous interacting magnetic elements, and characterization and control of their magnetic reversal is vital to proper operation, as many different forms of magnetic disorder are, in principle, possible.[6]

The concept of an order parameter is vital in modern physics for describing the behavior of large systems,[7] characterizing the state of the system by averaging over its microscopic details. This approach reflects the principle of scattering experiments where the entire sample is probed and averaged statistical quantities are extracted directly. A prototypical example is a ferromagnetic (FM) system, where the order parameter is the net magnetization defined as $\mathbf{M}=\langle\mathbf{m}(\mathbf{r})\rangle$, with $\langle\cdots\rangle$ denoting a spatial average over $\mathbf{r}$. Both in artificial multilayer materials and naturally occurring elements and compounds more complex forms of magnetic ordering can be found, requiring further order parameters to be defined, and experimental techniques must be found that can measure them. For instance, the traditional technique used to measure the antiferromagnetic (AF) order parameter of a crystal, often referred to as the staggered magnetization, is neutron diffraction.

While there have been tremendous advances in the resolution of electron and scanning probe microscopy for investigating surfaces, internal structures are determined (without destroying the sample) by electron, neutron or photon scattering techniques. Although photons comprise both oscillating electric and magnetic fields, x-ray scattering from matter is generally dominated by the Thomson charge scattering, with any magnetic signal being extremely weak in comparison.[8] However by tuning the photon energy to match a suitable resonance a tremendous enhancement of the magnetic signal is possible,[9,10] and by employing extremely intense, tunable synchrotron radiation, the study of magnetic materials using x-ray scattering is becoming well established.[11] Although early work concentrated on diffraction from bulk crystals,[12] often of 4 or 5*f* series elements,[13,14] reflectometry from 3*d*-element thin film samples was soon developed,[15,16] and the first measurements of a coupled multilayer were reported by Tonnerre *et al.*[17] More recently the technique has been widely applied, for instance to examine magnetic ripple in Co/Cu multilayers,[18] spiral domain structures in $L1_0$ FePd films,[19] exchange springs in Fe/Gd multilayers,[20] and reversal modes in patterned permalloy dots.[21] These techniques complement the use of neutron reflectometry[22,23] but offer advantages in terms of source brightness and element specificity, and there are substantial theoretical efforts to complement the experimental progress—see for instance Refs. 24 and 25. In this paper we report on x-ray scattering experiments from magnetic multilayers where the spacer layer thickness has been chosen to give rise to antiferromagnetic coupling between neighboring

 

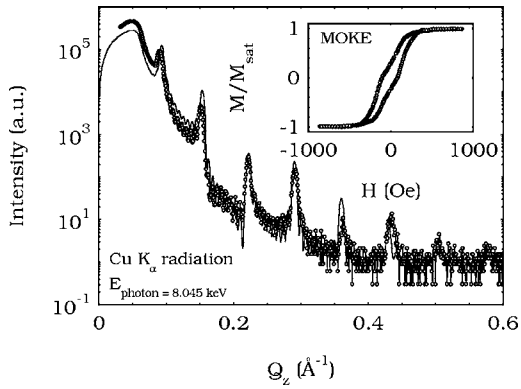


FIG. 1. Specular x-ray reflectivity spectrum of the Co/Ru multilayer measured with Cu $K_\alpha$ radiation. The points are experimental data while the solid line is a best fit using a dynamical model. The inset shows the room temperature hysteresis loop measured using the Kerr effect.

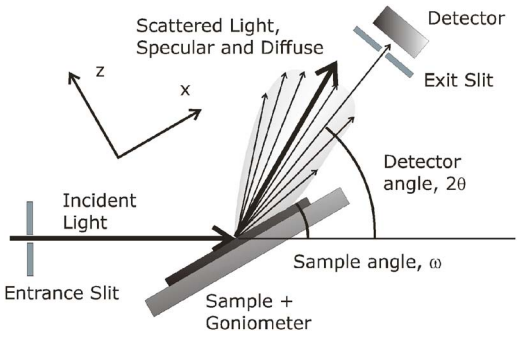


FIG. 2. (Color online) A sketch of the experimental geometry used. The $x$ and $z$ directions are defined with respect to the sample, and the magnetic field is applied along the $x$ axis. The point in reciprocal space probed is determined by the settings of the sample angle $\omega$ and the detector angle $2\theta$.

layers.[26] The high synchrotron flux and large magnetic signal means that we can measure the scattered intensity as a function of magnetic field, acquiring "hysteresis loops" in times of only a few minutes. The experimenter is free to choose the sample and detector positions, *viz.* a particular value of the wave-vector transfer **Q**, at which the loop is measured, and in this paper we will argue that different choices of **Q** give sensitivity to different magnetic order parameters within the sample. Antiferromagnetically ordered heterostructures are commonly used in spintronic devices to provide structures that present a large spin polarization at an external interface, but are stable against large field excursions as they possess no net magnetic moment.[27] Scattering methods such as this allow one to directly access this antiferromagnetic order as it will have a well-defined spatial frequency corresponding to a particular point in reciprocal space.

## II. SAMPLE PREPARATION AND CHARACTERIZATION

The samples we studied were deposited in a custom vacuum system (base pressure better than $2\times10^{-8}$ Torr) by dc magnetron sputtering. Multilayers with a nominal structure of {Co(58 Å)/Ru(30 Å)}$\times$10 were grown onto pieces of Si (001) wafer. The Ru thickness was chosen to correspond to the third antiferromagnetic coupling peak. The strong coupling in Co/Ru (Ref. 26) means that we can still find some useful antiferromagnetic coupling even at such large spacer thicknesses, which give Bragg features at fairly low values of **Q**, improving our counting statistics in scattering experiments. Structural characterization of the samples was carried out in the laboratory using Cu $K_\alpha$ radiation, while the magnetic properties were investigated with the magneto-optic Kerr effect (MOKE) using a HeNe laser. The macroscopic hysteresis loop of the sample, measured using MOKE, is shown in the inset of Fig. 1. The canted form of the loop confirms the presence of AF coupling of moderate strength. (Similar samples with appropriately thinner and thicker Ru layers showed more upright loops.) Although at weak interlayer coupling peaks the random anisotropy within each grain is the largest of the energy terms leading to the saturation field,[28] we can estimate the exchange constant $J\approx-0.05$ mJ/m$^2$, of about the correct magnitude for the third peak in the Co/Ru system.[29] Co/Ru is useful for our purposes as it is a well-understood model coupled multilayer system.

We define the coordinate system for scattering such that the $z$ direction lies normal to the sample, while the $x$ direction lies in both the sample and scattering planes. In all scattering experiments, our slit geometry means that variations in intensity in the $y$ direction are integrated out. Figure 1 shows the specular reflectivity spectrum for Cu $K_\alpha$ radiation. Several orders of multilayer Bragg peaks are clearly visible. Well-defined Kiessig fringes are also evident, indicating that the upper and lower surfaces of the multilayer stack are well correlated. The peak positions give the multilayer period as $\approx$87 Å, close to the nominal thickness. Measuring the full width at half-maximum (FWHM) of the peaks indicates that the multilayer structure is vertically coherent with a vertical structural correlation length $\sim$830 Å, approximately the total stack height. Fitting of the data using a distorted wave Born approximation model confirms the nominal layer thicknesses (according to the fit $t_{Co}=57\pm1$ Å and $t_{Ru}=32\pm1$ Å) and gives a typical interface roughness of $4\pm1$Å for a Co/Ru interface and $7\pm1$ Å for a Ru/Co one.

## III. SOFT XRMS RESULTS AND DISCUSSION

X-ray resonant magnetic scattering (XRMS) experiments were carried out at beamline U4B at the National Synchrotron Light Source, Brookhaven. This comprises a high resolution spherical grating monochromator and an ultrahigh vacuum end chamber containing a photodiode detector and a sample manipulator with a small electromagnet that allows steady fields of up to $\sim$300 Oe, and pulsed fields exceeding $\sim$1 kOe, to be applied to the sample along the $x$ axis. (We tuned the saturation field of our sample, through an appropriate choice of Co layer thickness, to give a value in line with these experimental constraints.) A sketch of our two-circle experimental geometry is shown in Fig. 2. In what

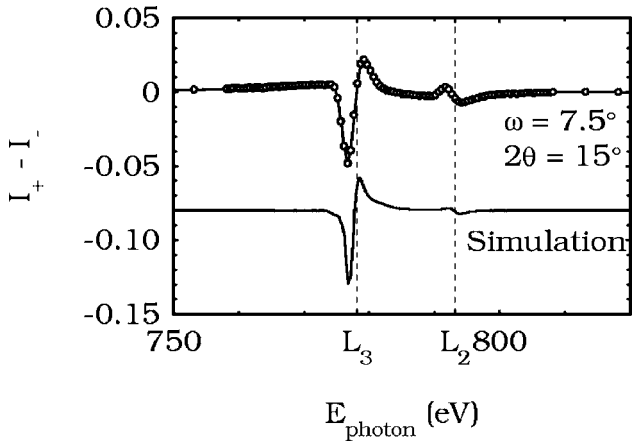


FIG. 3. Difference in specularly reflected intensity $I_+ - I_-$ for a fixed detector angle of 15° for the sample in two oppositely magnetized directions ($H = \pm 300$ Oe as a function of photon energy. The tabulated positions of the Co $L_3$ and $L_2$ edges (Ref. 32)are marked by the vertical dashed lines. The open circles show experimental data, while the solid line is a simulation using the model described in the text. The simulated curve is displaced vertically from the data. There is no particular significance to the choice of $2\theta = 15°$. We measured this curve for several different detector angles at the specular condition. Although differing slightly in the details, this curve is representative of them all.

follows we will refer to the sample angle as $\omega$ and the detector angle as $2\theta$, defined with respect to the incident beam. The choice of these two angles, along with the photon energy $E_{\text{photon}}$, defines the wave-vector transfer **Q** and hence the point in reciprocal space being probed. In this geometry the out-of-plane ($Q_z$) and in-plane ($Q_x$) components of the wave-vector transfer are given by the standard relationships,

$$Q_z = \frac{E_{\text{photon}}}{\hbar c}(\sin(2\theta - \omega) + \sin\omega), \tag{1a}$$

$$Q_x = \frac{E_{\text{photon}}}{\hbar c}(\cos(2\theta - \omega) - \cos\omega). \tag{1b}$$

All soft XRMS data presented have been normalized to the incident beam intensity, measured using a Au grid monitor mounted upstream of the entrance slits to the scattering chamber. Measurements with the shutter closed gave a low background count rate, associated with charged particles from the scatter chamber ion pump, indicating that we have a light-tight chamber. Typical chamber pressures during counting were $\sim 5 \times 10^{-8}$ Torr.

Energy scans of reflected intensity were performed to identify the resonances, which showed a small variation in the maximum signal energy with angle, of the order of a few eV. The difference in reflectivity for the positively and negatively magnetized sample $I_+ - I_-$, with photon energy for $2\theta = 15°$ is shown in Fig. 3. The solid line is a simulation using a magneto-optical model[30] that can be applied to reflectivity in the soft x-ray region.[31] The real part of the Co scattering factors used in the simulations were obtained from Kramers-Kronig transforms of the x-ray absorption and x-ray magnetic circular dichroism data measured from a sputtered Co thin film. Tabulated values were used for the (off-resonance) Ru scattering factors. The best-fit line was obtained by setting the Co and Ru layer thicknesses to 59 Å and 33 Å, respectively. The simulation reproduces the general features of the experimental curve well, although the relative intensities are slightly different. This small discrepancy is likely to be caused by imperfections in the multilayer structure, such as interface roughness, that are not included in the model. Since the absorption of the beam is heavy when exactly on resonance, all measurements were performed just off the tabulated Co $L_3$ resonance, with the photon energy set to 778 eV ($\lambda = 15.9$ Å). This represents the best balance between obtaining magnetic signal and maximizing the penetration depth of the x-ray photons so that a large volume of the sample is probed. The degree of circular polarization of the light was ~70 percent, with the remainder linearly polarized in the $y$ direction.

An initial rapid survey was undertaken to confirm the positions of the multilayer Bragg peaks along the specular ridge. The different real parts of the refractive index for circularly polarized light in the two oppositely magnetized states of the sample (that give rise to Faraday and Kerr rotations) leads to a slightly different position for the Bragg peak in $Q_z$ for the scans at forward and reversed fields. This dynamical splitting means that the difference of the two curves has a peak-derivative form at each Bragg peak with positive and negative going parts superimposed on the positive hump. (The fact that all peaks have a background signal of the same sign is often taken to mean that the magnetization profile within each layer is vertically uniform.[20]) The dynamical splitting is most pronounced at low order peaks and is barely visible by the fourth order peak, the highest we measured. Rocking curves ($\omega$ scans) were then performed with $2\theta$ set to integer and half-integer multiples of 10.6°, satisfying each Bragg and half-Bragg condition as closely as possible. During each scan the scattered intensity was measured at forward and reversed fields of the same magnitude for each setting of $\omega$. Pulsed fields of ~1500 Oe and 0.5 s duration were applied before the steady field was set to ensure that we remain on the major hysteresis loop of the sample for all measurements. Following the methods of earlier work, we measure the scattered intensity for the sample magnetized in two opposite directions and plot the sum and difference of the two values.[33,34] Subsequently developed theory shows that in this case sum data is a measure of purely structural or magnetic correlations (although the latter is very weak by comparison), while the difference measures cross correlations between the structure and magnetism.[35–37]

Narrow rocking scans around the specular position reveal the magnetic detail. The need to measure magnetic signals at small values of $Q_x$ show that the magnetically coherent regions are large in real space, they are ~$\mu$m sized. Scans were performed with forward and reverse fields of 300 Oe in the same sense as the high field pulse (saturation) and 120 Oe in the opposite direction to the pulse (coercivity). The results with $2\theta$ set to the Bragg conditions $n = 2$ and $n = \frac{5}{2}$ are shown in Fig. 4. In all cases the pairs of scans with the sample magnetized in opposite directions are rather

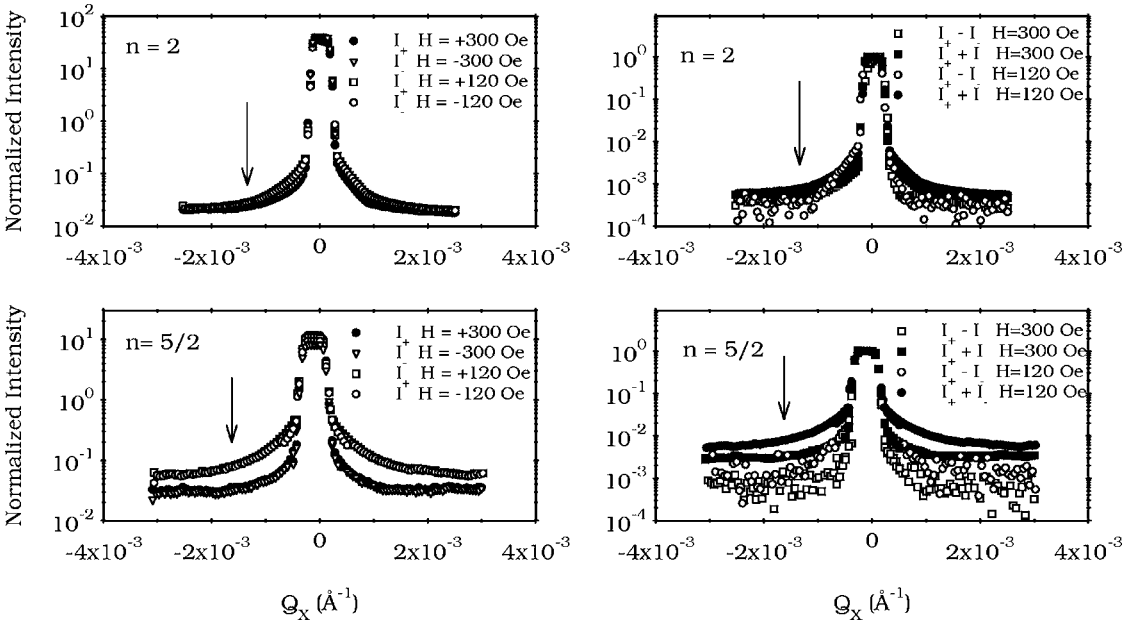


FIG. 4. Narrow rocking curves through the specular position for an integer ($n=2$) and half $\left(n=\frac{5}{2}\right)$ order Bragg peak position. On the left curves for four different fields are shown, ±300 Oe, a saturating field; and ±120 Oe, roughly the coercive field. On the right the average and difference plots are shown for the two different field values, normalized to the specular reflectivity. Higher levels of diffuse scatter are evident at 120 Oe, in particular at the $n=\frac{5}{2}$ position, where the sensitivity to AF ordering in the multilayer is highest. The arrows indicate the off-specular positions where hysteresis loops shown in Fig. 5 were recorded, measurements were also made at the specular position $Q_x=0$. It is worth making a comment here about the accuracy of our data, since the difference signal is a small difference of two large numbers. The level of noise in the various scans gives an indication of the degree of uncertainty in the data, visible only when the signal is close to the background. The uncertainty in the difference signal on the specular ridge is less than one part in $10^3$ and is at least one part in $10^2$ over most of the diffuse part of the scan as well.

similar. On going from the saturating to the coercive field, the rise in diffuse scatter at the half-order peak position is much greater than that at the integer position, even in the sum data. It can be seen that even after averaging over the different helicities of the light a sensitivity to magnetism remains. This diffuse scatter is the sign of substantial AF coupling in the multilayer at this position, giving rise to substantially more scattered intensity than the formation of domains during magnetization reversal. An odd feature is that the formation of AF order causes the diffuse intensity to rise by roughly half an order of magnitude, while very little change can be discerned in the specular intensity—measurement of specular scans only does not directly reveal the presence of AF ordering in this particular instance. This type of effect has been previously observed using linearly polarized light,[38] although it remains difficult to explain. (We note paranthetically that this peculiar effect seems to depend on the materials system used, possibly reflecting the details of the domain state of the AF order formed. We have previously measured strong specular half-order peaks in Co/Cu using soft XRMS,[18] but the Fe/Cr and Co/Ru samples studied in Ref. 38 do not exhibit them. Tonnerre *et al.* observed a specular half-order peak from Ni/Ag.[17] In this paper we again used Co/Ru. Half-order intensity is found in all these systems when PNR was employed,[6,38–40] as it is in longitudinal diffuse scans performed using soft XRMS. In a recent report from Spezzani *et al.* only a weak half-order peak was discerned in scattering from a Co/Cu multilayer in the specular scan while it was much stronger in the longitudinal diffuse.[41] We will publish more fully on this phenomenon elsewhere.)

We now come to discuss the most important of our experimental results. Here both $\omega$ and $2\theta$ were set to select a particular point in reciprocal space, and the intensity measured as as function of applied field, a similar procedure to that employed by Spezzani *et al.*,[42,43] although in this case we have also collected data in off-specular positions in reciprocal space. Figure 5 shows the results of carrying out this procedure for structural Bragg and anti-Bragg positions $n=2$ and $n=\frac{5}{2}$, with $\omega$ set to $\theta$ or $\theta-0.5°$. This offset angle will be denoted by $\Delta\omega$. Again, before each sweep a high field pulse was applied to the sample to ensure that we remain on the major hysteresis loop. It is immediately apparent that a variety of different shapes are observed for different settings of $\omega$ and $2\theta$, and hence different choices of $\mathbf{Q}$. The variations in scattered intensity above the baseline intensity reflect the changes in the various types of magnetic ordering driven by the varying field.

Let us begin by examining the loops measured at the specular condition, $Q_x=0$. Using the language of traditional hysteresis loops, the loops measured for $\Delta\omega=0$ at $n=2$ and $n=3$ are canted with low coercive fields, low remanences and high saturation fields. That at $n=3$ is inverted is due to the dynamical part of the dichroism signal giving a different overall sign relative to the $n=2$ position. In contrast the loops measured at $n=\frac{3}{2}$ and $n=\frac{5}{2}$ are much wider and squarer, with a much higher coercivity. Again these two loops are inverted with respect to the one at $n=2$ due to the

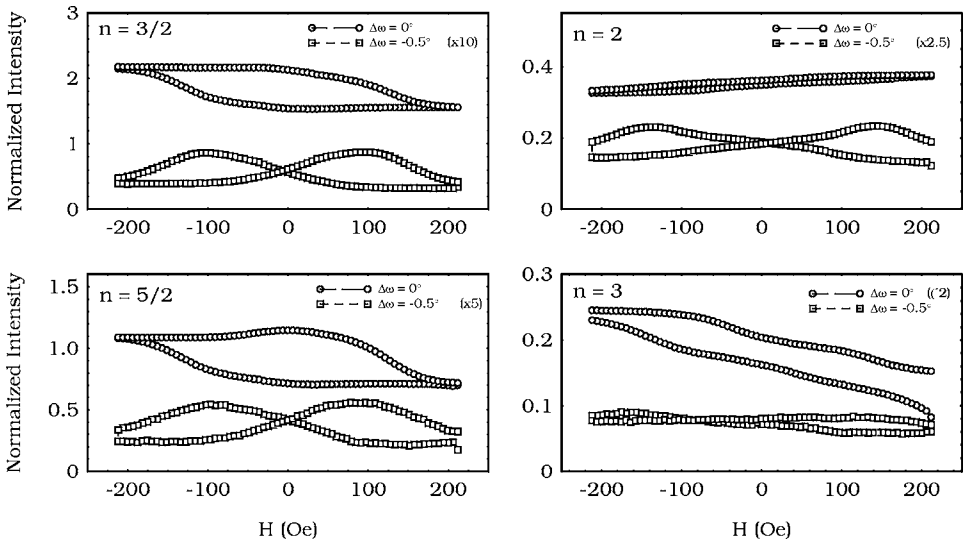


FIG. 5. Hysteresis loops of x-ray intensity measured with the apparatus set to be sensitive to scatter at different points in reciprocal space. Loops with offsets in $\omega$ of 0° (○), and −0.5° (□) are shown. The data for the specular position ($\Delta\omega=0$), $n=2$ loop appears rather compressed on this scale, but is reproduced in Fig. 6 more clearly.

sign of the dichroism at these values of **Q**. Turning our attention to the data measured at $\Delta\omega \neq 0$ we can see that the shape of the curve is entirely different, with a double peaked form. At these off-specular values of **Q** we are sensitive to in-plane structures such as domains, and the intensity peaks at fields where these form.

Of course in both the XRMS and Kerr experiments one is reflecting polarized light from the sample surface to probe magnetism, and under appropriate conditions one would expect to obtain very similar results. In Fig. 6 we plot the normalized XRMS loop for $n=2$ and $\Delta\omega=0$ and the normalized Kerr loop for the same sample. They agree in many of the important features of the curve, such as a slight wasp-waist, and reversal clearly occurs over the same field range. The detailed interpretation of the XRMS loop is complicated by the fact that the dynamical effects mentioned above also play a role in determining the intensity close to the Bragg condition. Due to the dynamical peak splitting, as one sweeps the field and reverses the sample magnetization at a fixed **Q** one can shift on and off the Bragg condition, distorting the shape of the loop somewhat. Nevertheless the broad agreement indicates that at this point in reciprocal space we are primarily sensitive to the macroscopic magnetization of the sample—alternatively it is equivalent to say that we are primarily sensitive to the ferromagnetic order parameter $M$. [Most XRMS hysteresis loops previously measured have assumed that this is true, see for instance Refs. 34 and 44 for examples measured on single films of CoFe.]

The different shapes of the other scans indicate that they reflect other forms of magnetic order. We would expect our sample to form an antiferromagnetic structure at low fields due to the choice of the Ru layer thickness. It is possible to define an antiferromagnetic order parameter, usually referred to as the staggered magnetization, to distinguish between AF ordered and disordered states that both have a ferromagnetic order parameter equal to zero. It is well known that the giant magnetoresistance (GMR) is sensitive to the degree of antiferromagnetic order in a multilayer, as it is $\propto\langle\cos\Theta\rangle$, with $\Theta$ the difference in angle between the magnetic moments in adjacent layers. However the GMR of Co/Ru is very small, typically much less than 1%.[45] Indeed, when magnetotransport measurements were made (at room temperature using a standard four-point probe dc technique), the data, displayed in Fig. 7(a), can be seen to be dominated by the anisotropic magnetoresistance (AMR). In order to extract the GMR from the data we can recall that the AMR $\sim\sin^2\theta$, where $\theta$ is the angle between the current density and the magnetization. Rotating the sample by 90° and measuring again will yield an AMR $\sim\cos^2\theta$, and the sum of the two measurements will be a constant if AMR is the only magnetoresistive effect present.[46] In fact an average of the two data sets, shown in Fig. 7(b), shows clear hysteretic peaks at ±90 Oe.

We can now compare this data with the XRMS hysteresis loops taken at $Q_x \neq 0$. The loops with a sample angle offset of $\Delta\omega=-0.5°$ at the $n=\frac{3}{2}$ and $n=2$ positions are shown in Fig. 7(c). The positions of the peaks in the $n=\frac{3}{2}$ data set align closely with those seen in the GMR data of panel (b), clearly identifying this intensity as being associated with antiferromagnetically coupled domains. The peaks in the $n=\frac{5}{2}$ loop are at the same field as in the $n=\frac{3}{2}$ loop to within the point spacing, 6 Oe, indicating that these domains are highly vertically coherent. (This vertical coherence is commonplace in these coupled multilayer structures, see the neutron data

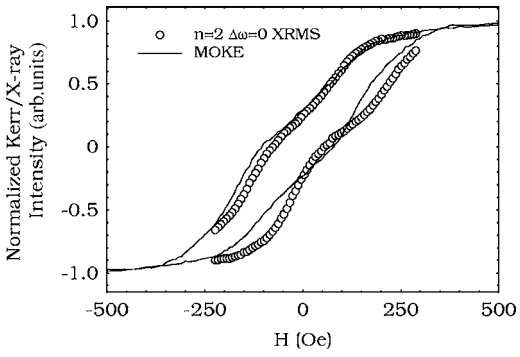


FIG. 6. A superposition of the normalized Kerr hysteresis loop (solid line) and the $n=2$ specular loop measured by XRMS (○). Although there are distortions in the loop shape due to the dynamical variations in the scattered intensity with field, the broad agreement is evident.

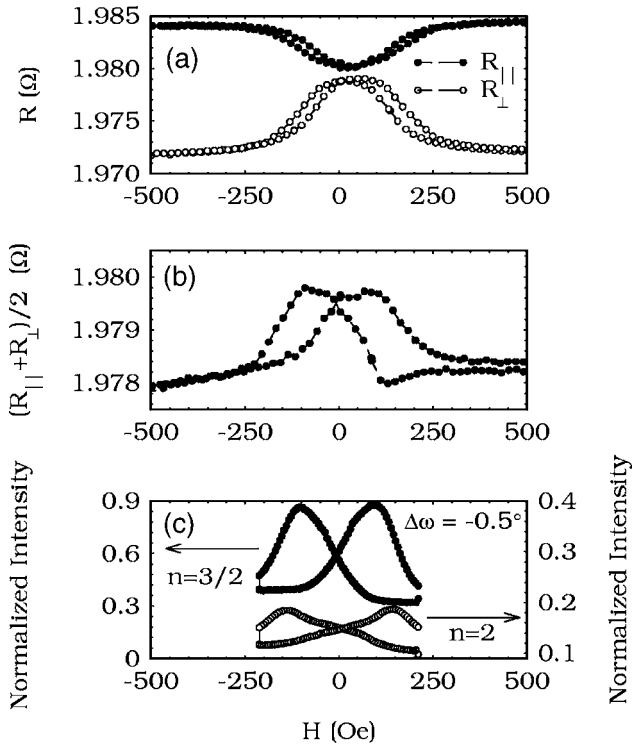


FIG. 7. (a) Magnetoresistance measurements of the sample in the longitudinal ($R_{\parallel}$, ●) and transverse ($R_{\perp}$, ○) geometries. The results are dominated by the AMR. (b) The average of the two transport data sets, $(R_{\parallel}+R_{\perp})/2$, showing hysteretic peaks at ±90 Oe. (c) The XRMS data at an offset angle of $\Delta\omega=-0.5°$ for $n=\frac{3}{2}$ and $n=2$. Only the peaks measured at the half-order positions align with the data in panel (b).

in Refs. 6, 39, and 47 for examples. It is also observed in domain imaging experiments, see for instance Ref. 48 where Lorentz microscopy was used to image an antiferromagnetically coupled Co/Cu multilayer.) As the reverse field is made larger, this intensity at half-order begins to fall off and that at the $n=2$ off-specular position rises. The peaks in this data, also shown in Fig. 7(c), occur at $H=\pm 150$ Oe, showing that the magnetization within the domains is now predominantly ferromagnetically aligned at these higher fields. This intensity also falls away as the domains are swept out of the sample in the approach to saturation. The off-specular data for other values of $n$ and $\Delta\omega$ show peaks at similar fields and confirms this picture of the magnetization reversal. We can therefore identify the intensity measured at the off-specular multilayer positions as dominated by antiferromagnetic (for half-order) and ferromagnetic (for integer order) vertical correlations within the domains.

It can be seen that this intensity falls to rather a low value for fields approaching saturation regardless of the value of $Q_z$, indicating that both structural and magnetic roughness contributions are comparatively low. The intensity at the peaks is dominated by the field dependent part, which must be related to domain formation as it must be some magnetic feature that has inhomogeneities over the sample plane. These loops are thus the measure of the value of the FM or AF order parameter (true or staggered multilayer magnetization) when it varies locally over regions of lateral size smaller than $\sim 2\pi/Q_x$. Real space features of a larger size will only give rise to intensity close to the specular ridge and will contribute little at these values of $Q_x$. For the plots in Fig. 7(c) these sizes are $\sim 0.61$ $\mu$m for the $n=\frac{3}{2}$ loop and $\sim 0.47$ $\mu$m for the $n=2$ loop. This characteristic length scale that is probed can be chosen by the experimenter by selecting the value of $Q_x$ at which the measurement is performed. A brief survey at other values of $\Delta\omega$ showed that in this particular sample the fields at which the peaks in the diffuse scatter appeared did not depend on $Q_x$, only on whether an integer or half-integer Bragg peak is selected. This leads us to the conclusion that the degree of antiferromagnetic (or ferromagnetic) order within a domain is not related to its size in this sample. The in-plane coherence length of the x-ray beam is $\sim\lambda^2/2\Delta\lambda$,[49] for $\lambda=15.9$ Å and a resolving power of a few thousand provided by the monochromator[50] we can anticipate this length to be a few $\mu$m, even after accounting for the foreshortening at finite sample angles. This length will also limit the maximum size of domains that can be detected by this method, but exceeds the length scales here by roughly an order of magnitude.

The most difficult loops to interpret are those measured at specular half-order positions. As stated above there are no obvious half-order specular peaks, and so the AF contribution to the intensity at this point is rather weak compared to the FM contribution that affects the whole specular ridge. Nevertheless the shape is significantly different when compared to a loop measured at an integer-order position. It is evident that at this position, despite the absence of a clear Bragg peak, the AF order plays a role in determining the scattered intensity. A simple qualitative explanation is that when AF order is high (around the true coercive fields, i.e., the ones defined on the basis of a conventional hysteresis loop) this will lead to additional scattering which compensates for the falling intensity associated with the FM order. This will give a higher apparent "remanence" and a more rapid drop as the AF order disappears at higher reverse fields. This will cause the canted loop to bulge outwards, giving the wider, squarer appearance. Much of the intensity generated at this $Q_z$ at fields corresponding to high AF order is not to be found on the specular ridge but in diffuse positions at $Q_x \neq 0$.

In the past differences in hysteresis loops obtained at the specular and diffuse positions have been attributed to a slightly higher coercivity for the surface magnetism,[34] although this is difficult to reconcile with exchange fields coupling the surface to the bulk that are strong enough to give ferromagnetic order at room temperature. Our results suggest a possible alternative explanation—that the higher apparent coercivity is due to a mixing in of the domain disorder term at diffuse positions, which peaks at $H_c$, subtly distorting the shape of the loop. This point deserves further detailed investigation.

## IV. IN CONCLUSION

We have carried out XRMS measurements using soft x-rays on a magnetic multilayer system containing various forms of magnetic order and disorder. By choosing the

configuration of our scattering apparatus to give sensitivity to correlations at different points in reciprocal space it is possible to measure hysteresis loops with a rich variety of different shapes. By comparing our XRMS loops to hysteresis loops measured my different macroscopic techniques, these shapes have been related to the various components of the ferromagnetic and antiferromagnetic order parameters describing the magnetism of the sample. We have given detailed, albeit sometimes qualitative arguments to support these comparisons. The details of the quantitative model required to relate these to the various positions in **Q** space are an outstanding challenge to theory and the development of a complete dynamical model will be worthwhile, as in principle a complete characterization of the reversal modes of magnetic nanostructures is possible by this method.

## ACKNOWLEDGMENTS

The authors would like to acknowledge Brookhaven National Laboratory for the provision of NSLS beamtime, the ONRIFO for travel support and the EPSRC for financial support.

*Electronic mail: c.h.marrows@leeds.ac.uk
†Present address: Diamond Light Source, Rutherford Appleton Laboratory, Chilton, Didcot, Oxon, OX11 0QX United Kingdom.

[1] F. J. Himpsel, J. E. Ortega, G. J. Mankey, and R. F. Willis, Adv. Phys. **47**, 511 (1998).
[2] D. Weller and M. F. Doerner, Annu. Rev. Mater. Sci. **30**, 611 (2000).
[3] R. Coehoorn, *Magnetic Multilayers and Giant Magnetoresistance*, Vol. 37 of Springer Series in Surface Sciences (Springer, Berlin, 1999), Chap. 4, p. 65.
[4] S. Tehrani *et al.*, Proc. IEEE **91**, 703 (2003).
[5] *Spin Electronics*, edited by M. Ziese and M. J. Thornton, Lecture Notes in Physics (Springer, Berlin, 2001).
[6] S. Langridge, J. Schmalian, C. H. Marrows, D. T. Dekadjevi, and B. J. Hickey, Phys. Rev. Lett. **85**, 4964 (2000).
[7] P. M. Chaikin and T. C. Lubensky, *Principles of Condensed Matter Physics* (Cambridge University Press, Cambridge, 1995).
[8] F. de Bergiven and M. Brunel, Acta Crystallogr., Sect. A: Cryst. Phys., Diffr., Theor. Gen. Crystallogr. **37**, 314 (1981).
[9] J. P. Hannon, G. T. Trammell, M. Blume, and D. Gibbs, Phys. Rev. Lett. **61**, 1245 (1988).
[10] S. W. Lovesey and S. P. Collins, *X-Ray Scattering and Absorption by Magnetic Materials*, Oxford Series on Synchrotron Radiation (Oxford University Press, Oxford, 1996).
[11] G. H. Lander, J. Magn. Magn. Mater. **242**, 3 (2002).
[12] K. Namikawa, M. Ando, T. Nakajima, and H. Kawata, J. Phys. Soc. Jpn. **54**, 4099 (1985).
[13] D. Gibbs, D. R. Harshman, E. D. Isaacs, D. B. McWhan, D. Mills, and C. Vettier, Phys. Rev. Lett. **61**, 1241 (1988).
[14] E. D. Isaacs, D. B. McWhan, C. Peters, G. E. Ice, D. P. Siddons, J. B. Hastings, C. Vettier, and O. Vogt, Phys. Rev. Lett. **62**, 1671 (1989).
[15] C. Kao, J. B. Hastings, E. D. Johnson, D. P. Siddons, G. C. Smith, and G. A. Prinz, Phys. Rev. Lett. **65**, 373 (1990).
[16] C. Kao *et al.*, Phys. Rev. B **50**, 9599 (1994).
[17] J. M. Tonnerre, L. Sève, D. Raoux, G. Soullié, B. Rodmacq, and P. Wolfers, Phys. Rev. Lett. **75**, 740 (1995).
[18] T. P. A. Hase, I. Pape, B. K. Tanner, H. Dürr, E. Dudzik, G. van der Laan, C. H. Marrows, and B. J. Hickey, Phys. Rev. B **61**, R3792 (2000).
[19] H. A. Dürr, E. Dudzik, S. S. Dhesi, J. B. Goedkoop, G. van der Laan, M. Belakhovsky, C. Mocuta, A. Marty, and Y. Samson, Science **284**, 2166 (1999).
[20] N. Ishimatsu, H. Hashizume, S. Hamada, N. Hosoito, C. S. Nelson, C. T. Venkataraman, G. Srajer, and J. C. Lang, Phys. Rev. B **60**, 9596 (1999).
[21] C. Spezzani, M. Fabrizioli, P. Candeloro, E. Di Fabrizio, G. Panaccione, and M. Sacchi, Phys. Rev. B **69**, 224412 (2004).
[22] G. P. Felcher and S. G. E. te Velthuis, Appl. Surf. Sci. **182**, 209 (2001).
[23] H. Zabel and K. Theis-Bröhl, J. Phys.: Condens. Matter **15**, S505 (2003).
[24] D. R. Lee, S. K. Sinha, D. Haskel, Y. Choi, J. C. Lang, S. A. Stepanov, and G. Srajer, Phys. Rev. B **68**, 224409 (2003).
[25] D. R. Lee, S. K. Sinha, C. S. Nelson, J. C. Lang, C. T. Venkataraman, G. Srajer, and R. M. Osgood III, Phys. Rev. B **68**, 224410 (2003).
[26] S. S. P. Parkin, Phys. Rev. Lett. **67**, 3598 (1991).
[27] C. H. Marrows, F. E. Stanley, and B. J. Hickey, Appl. Phys. Lett. **75**, 3847 (1999).
[28] D. J. Kubinski and H. Holloway, J. Appl. Phys. **82**, 322 (1997).
[29] S. S. P. Parkin, N. More, and K. P. Roche, Phys. Rev. Lett. **64**, 2304 (1990).
[30] J. Zak, E. R. Moog, C. Liu, and S. D. Bader, J. Magn. Magn. Mater. **89**, 107 (1990).
[31] J. B. Kortright and S.-K. Kim, Phys. Rev. B **62**, 12216 (2000).
[32] http://xdb.lbl.gov
[33] J. F. MacKay, C. Teichert, D. E. Savage, and M. G. Lagally, Phys. Rev. Lett. **77**, 3925 (1996).
[34] J. W. Freeland, K. Bussmann, P. Lubitz, Y. U. Idzerda, and C.-C. Kao, Appl. Phys. Lett. **73**, 2206 (1998).
[35] R. M. Osgood III, S. K. Sinha, J. W. Freeland, Y. U. Idzerda, and S. D. Bader, J. Appl. Phys. **85**, 4619 (1999).
[36] R. M. Osgood III, S. K. Sinha, J. W. Freeland, Y. U. Idzerda, and S. D. Bader, J. Magn. Magn. Mater. **199**, 698 (1999).
[37] C. S. Nelson, G. Srajer, J. C. Lang, C. T. Venkataraman, S. K. Sinha, H. Hashizume, N. Ishimatsu, and N. Hosoito, Phys. Rev. B **60**, 12234 (1999).
[38] T. P. A. Hase, J. D. R. Buchanan, B. K. Tanner, S. Langridge, R. M. Dalgliesh, S. Foster, C. H. Marrows, and B. J. Hickey, J. Appl. Phys. **93**, 6510 (2003).
[39] S. Langridge, J. Schmalian, C. H. Marrows, D. T. Dekadjevi, and B. J. Hickey, J. Appl. Phys. **87**, 5750 (2000).
[40] S. Langridge, C. H. Marrows, and P. Steadman (unpublished).

[41] C. Spezzani, P. Torelli, R. Delaunay, C. F. Hague, F. Petroff, A. Scholl, E. M. Gullikson, and M. Sacchi, Physica B **345**, 153 (2004).
[42] C. Spezzani, P. Torelli, M. Sacchi, R. Delaunay, C. F. Hague, V. Cros, and F. Petroff, Appl. Phys. Lett. **81**, 3425 (2002).
[43] C. Spezzani, P. Torelli, M. Sacchi, R. Delaunay, C. F. Hague, F. Salmassi, and E. M. Gullikson, Phys. Rev. B **66**, 052408 (2002).
[44] J. W. Freeland, V. Chakarian, K. Bussmann, Y. U. Idzerda, H. Wende, and C.-C. Kao, J. Appl. Phys. **83**, 6290 (1998).
[45] M. Perez, C. H. Marrows, and B. J. Hickey, J. Appl. Phys. **89**, 7116 (2001).
[46] M. Viret, D. Vignoles, D. Cole, J. M. D. Coey, W. Allen, D. S. Daniel, and J. F. Gregg, Phys. Rev. B **53**, 8464 (1996).
[47] C. H. Marrows, S. Langridge, M. Ali, A. T. Hindmarch, D. T. Dekadjevi, S. Foster, and B. J. Hickey, Phys. Rev. B **66**, 024437 (2002).
[48] C. H. Marrows, B. J. Hickey, M. Herrmann, S. McVitie, J. N. Chapman, M. Ormston, A. K. Petford-Long, T. P. A. Hase, and B. K. Tanner, Phys. Rev. B **61**, 4131 (2000).
[49] J. Als-Nielsen and D. McMorrow, *Elements of Modern X-Ray Physics* (Wiley, New York, 2001).
[50] http://www.nsls.bnl.gov/beamlines/beamline.asp?blid=u4b